



# Analysing the light-to-heat conversion of Black Carbon agglomerates to interpret results from different light absorption instruments

Nikolaos Kousias<sup>1</sup>, Ioannis Raptis<sup>1</sup>, Linda Haedrich<sup>2,3</sup>, Vasilis Ntziachristos<sup>2,3,4</sup>, Leonidas Ntziachristos<sup>1</sup>

- <sup>1</sup> Mechanical Engineering Department, Aristotle University of Thessaloniki, Box 458, 54124, Thessaloniki, Greece
- <sup>2</sup> Chair of Biological Imaging at the Central Institute for Translational Cancer Research (TranslaTUM), School of Medicine, Technical University of Munich, 81675, Munich, Germany
  - <sup>3</sup> Institute of Biological and Medical Imaging, Helmholtz Zentrum München, 85764, Neuherberg, Germany
  - <sup>4</sup> Munich Institute of Robotics and Machine Intelligence (MIRMI), Technical University of Munich, 80992, Munich, Germany *Correspondence to*: Leonidas Ntziachristos (leon@auth.gr)
- Abstract. Black Carbon (BC) is an important pollutant due to its climatic and health effects. Most BC detection devices rely on light absorption but measured BC concentrations may vary due to different light settings. Here, we propose a theoretical model that can be used to interpret and correct the signal of optoacoustic devices. It is based on Laser Induced Incandescence (LII) theory, but advancing the description of light absorption and heat conduction by agglomerate particles. It is validated with existing experimental literature data and with new optoacoustic measurements. The model predicts that high fractal dimensions are associated with weaker signal and that the volume to surface ratio can be used as a signal reduction predictor. Then, we introduce a dimensionless metric which very well corelates with the measured signal from BC particles. The new metric can be used to harmonize measurements from different devices and also extract particle morphological information from optoacoustic signals.

## 1 Nomenclature

a	Particle relaxation exponent	$\mathrm{M}_{\lambda}$	Blackbody spectral radiation
$a_{th}$	Particle thermal accommodation coefficient	MAC	Mass Absorption Cross-section
BC	Black Carbon	$N_p$	Number of primary particles in agglomerate
$C_{BC}$	Particle heat capacity	OA	Optoacoustic
$C_p$	Air specific heat capacity	OT	Optothermal
$c_s$	Speed of sound	$P_{g}$	Air pressure
D	Spherical particle diameter	$Q_{abs}$	Absorption coefficient of particle
$\mathrm{D_{f}}$	Agglomerate particle / Fractal dimension	$Q_c$	Continuum regime heat conduction
$D_{g}$	Agglomerate particle / Diameter of gyration	Qcond	Particle evaporation ratio
$d_{pp}$	Agglomerate particle / Primary particle diameter	$Q_{\mathrm{fm}}$	Free-molecular regime heat conduction
$\mathrm{DH}_{\mathrm{v}}$	Vaporization enthalpy of BC particle	q(t)	Light beam modulation pulse
$E_{m}$	Experimental refractive index function	R	Gas constant for air
$f_c$	Factor for convergence	$T_{OA}$	Dimensionless metric for OA signal
$f_{\text{mod}}$	Modulation frequency	$T_{g}$	Air temperature
FFT	Fast Fourier Transform	$T_p$	Particle temperature
$k_{\mathrm{B}}$	Boltzmann constant	$T_{rel}$	Particle relaxation time
$\mathbf{k}_{\mathrm{f}}$	Agglomerate particle / Fractal pre-factor	β	Air thermal expansion coefficient





k<sub>g</sub> Air heat conduction coefficient

Kn Knudsen number

LII Laser Induced Incandescence

m<sub>g</sub> Average mass of a gas molecule

M<sub>v</sub> Molar mass of BC vapor

 $\gamma^*$  Average specific heat ratio of air for large  $\Delta T$ 

 $\varepsilon_{\lambda}$  Emissivity of particle at wavelength  $\lambda$ 

λ Radiation wavelength

ρ<sub>BC</sub> Particle density

ω Modulation angular frequency

#### 20 1 Introduction

30

45

Black Carbon (BC) is a significant pollutant due to its adverse health effects (Janssen et al., 2011; World Health Organization, 2012) and its strong light absorption, which leads to climate forcing (Bond et al., 2013; Dou and Xiao, 2016). Technologies that rely on light absorption for BC detection, such as the optoacoustic (OA) and optothermal (OT) ones and Laser Induced Incandescence (LII), are essential in developing policies that aim to limit the effect of BC on climate (Clean Air Coalition 2014). BC varies in its chemical composition and properties, based on the emission source and on its mixing state after emission. The ability to extract more information from OA, OT and LII sensors can aid the characterization and source apportionment of BC. Moreover, harmonization tools are needed to compare BC measurements from different instruments or from the same instrument when measuring a different particle mix. Modelling work can also aid the extraction of additional information from ambient BC samples and be used to harmonize different measurements.

Specific OA models exist to describe the absorption of optical energy and the generation of the acoustic signal when light is absorbed by gases (Kosterev et al., 2006; Wysocki et al., 2006). However, the relevant mechanisms for gases are not readily applicable to particles. Models for particles mostly emphasize on two aspects: the generation of acoustic waves from specific excitation (Diebold and Westervel, 1988; Fujii et al., 2022) and the acoustic properties of a cavity (Baumann et al., 2007; Cotterell et al., 2019; Zhou, 2019). Such models can provide significant input – e.g. for optimizing an OA instrument – but cannot be used to provide information on particle properties, neither to contribute towards measurement standardization. The light-to-heat processes for particles need first to be described before an OA signal can be used for interpretation of particle properties.

An analysis of the heat conduction from particles for OA sensors was performed by Pustovalov (2016), but it is limited to individual spherical nanoparticles and nanoparticle assemblies, with emphasis on metal particles. Imran & Hochgreb (2019) developed a model for both spherical and agglomerate BC particles but did not analyse the effect of particle morphology on the OA signal. Ajtai et al. (2023) experimentally identified an effect of particle morphology on the phase of the OA signal, with larger particles demonstrating reduced phase. Ajtai et al. (2023) using the models of Moosmüller et al. (2009) highlighted the deviation of existing models from experimental results and recommended that an improved theory is needed. Such an improved theory can be based on a detailed analysis of an energy dissipation model for OA, similar to the ones used for LII.

Dissipation of energy from BC particles has been analysed in detail for LII sensors. Michelsen (2003) and Michelsen et al. (2015) presented an elaborate model that includes several dissipation mechanisms for BC particles. Hadef et al. (2010) presented a simpler version with the most relevant mechanisms for LII sensors. Snelling et al. (2004) used a similar model and performed an experimental evaluation to fine-tune the heat conduction term. Starke et al. (2003) developed an algorithm that

https://doi.org/10.5194/egusphere-2025-4498 Preprint. Discussion started: 27 November 2025





50

55

65



can calculate the average particle size based on the delay of the LII signal. In addition, Meyer et al. (2016) showed that 3D images of BC particles can be constructed from LII signal analysis. Willems et al. (2019) developed a model that combine signals from LII and OA sensors. However, the dissipation mechanisms are only used for the LII sensor, and the OA signal is used as an independent additional input. A theoretical model that applies similar LII energy dissipation mechanisms of BC particles for OA sensors is still missing.

In this work, we present for the first time an analytical model that can predict the signal intensity from BC particle samples for a given incipient light source, and we incorporate a method to estimate the broadband acoustic response for given light modulation. We have implemented the model for particles of different morphology, and we observed that the volume over surface ratio of an agglomerate BC particle can affect the intensity of the generated OA signal. The model can be used to extract morphological characteristics of BC particle samples and help identify their source, and can guide relevant instrument development. A modified version of the proposed model has the potential to assist in the design of OT sensors as well.

#### 2 Methodology

#### 2.1 Model conceptual formulation

Figure 1 outlines the main mechanisms for OA signal generation from a BC particle. Figure 1a shows the mechanisms for an agglomerate particle, and Fig. 1b shows the same mechanisms for a spherical particle, assuming both particles are of the same mass. Based on the particle's Mass Absorption Cross-section (MAC) the mass is translated to an amount of absorbed light for given excitation. For the example of Fig. 1, we may also assume that the particles have the same MAC and thus the amount of absorbed light ( $I_1$ ,  $I_2$ ) is the same for both the agglomerate and the spherical particle. In reality, the assumption of constant MAC is not valid for spherical particles larger than roughly 150 nm for visible light excitation (Jennings and Pinnick, 1980). For BC agglomerates, the assumption of constant MAC is valid, as the limit of 150 nm applies on the diameter of the primary particles, which is typically much lower. In any case, understanding the relation of MAC to particle size is not the focus of the current analysis. The same refractive index, which is the main parameter that affects MAC, is used for the entire analysis.

Next comes the modelling of light-to-heat processes, in order to calculate the amount of energy that is transferred to the surrounding air by heat conduction ( $H_1$ ,  $H_2$ ). This is the energy source for the OA signals, which actually constitutes the main focus of the current work. Our hypothesis is that the heat conduction profile is not the same for a spherical and an agglomerate particle of the same mass. Specifically, we argue that spherical particles will have a smaller amplitude of heat flux to the surrounding air than an agglomerate with the same mass that has absorbed the same amount of light. As the intensity of the generated acoustic waves ( $P_1$ ,  $P_2$ ) is proportional to the amount of heat conduction, we expect that the acoustic wave will also be weaker for the spherical particle compared to the agglomerate one. We assume that this difference will be explained by the higher surface to volume ratio of the agglomerate particle.





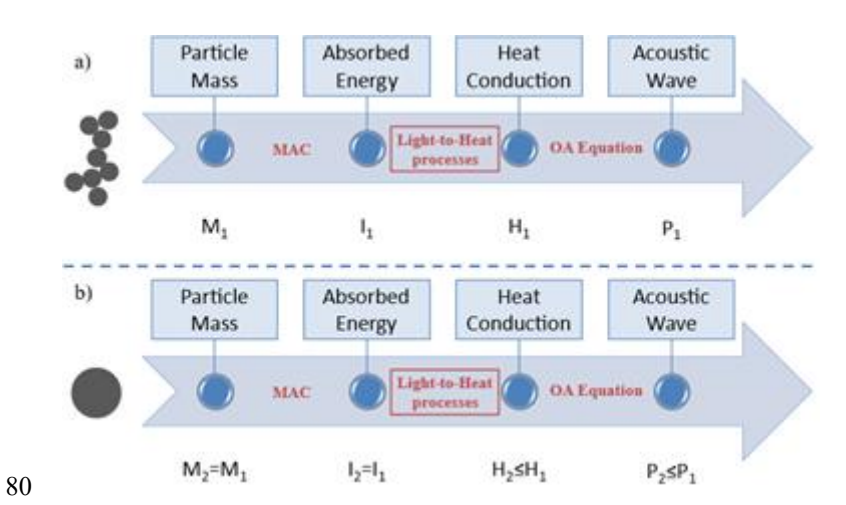


Figure 1: Conceptual model of particle light absorption to acoustic wave generation for (a) an agglomerate and (b) a spherical particle of the same mass.

#### 2.2 Model formulation

85

90

95

100

We use an energy balance model to simulate the light-to-heat processes for BC particles, following the principles of the models developed for LII applications. In particular, the model of Hadef et al. (2010) is used as a basis for the current analysis. The basic parameters of such a model are shown in Eq. (1) for a single particle. The term on the left side of Eq. (1) is the internal energy of the particle, which is function of its temperature. On the right side, the first term stands for light absorption, the second one for particle vaporization (sublimation), the third one for heat loss (conduction) from the particle to the surrounding air, and the fourth one for blackbody radiation. For both OA and OT applications, the most important terms are absorption, heat conduction and the particle's internal energy. Radiation and sublimation are only relevant at higher temperatures, which are typical for LII but which are not reached in OA and OT applications.

$$\rho_{BC}C_{BC}\frac{\pi D^3}{6}\frac{dT_p}{dt} = Q_{abs}\frac{\pi D^2}{4}q(t) + \frac{\Delta H_v}{M_v}\frac{dm}{dt} - \dot{Q}_{cond} - \pi D^2 \int_0^\infty \varepsilon_{\lambda} M_{\lambda} d\lambda \tag{1}$$

In the current work, the model of Hadef et al. (2010) was further extended by considering particles as being agglomerate structures instead of spheres. Moreover, Hadef et al. (2010) calculates the particle absorption efficiency ( $Q_{abs}$ ) by using particle size, light wavelength, and an experimental absorption function  $E_m$  as inputs. In our model, instead of relying on the experimentally determined function  $E_m$ , we explicitly calculate the absorption efficiency based on particle refractive index, making the process adaptable to particles of different properties. Finally, we calculate the heat conduction term with a process that can be applied to all molecular regimes (free-molecular, transition, and continuum), instead of the expression proposed by Hadef et al. (2010), which is only applicable to the free-molecular one. This also extends the model, beyond primary spherules to fully grown agglomerates, as typical atmospheric BC particles are. The radiation and sublimation terms are included in the initial calculations to investigate the limits of modulation for optimal OA signal generation. The terms are negligible in all subsequent simulations, and we introduced no improvements for them.



105

110

120

125

130



In OT sensors, the heat conducted by the particle to the surrounding air is directly proportional to signal intensity. In OA sensing, an additional step is required to convert the conducted heat to a pressure wave, as incoming light to the particle is modulated. The method proposed should be applicable to any light shape modulation (e.g. rectangular pulses) so the overall heat conduction profile is converted to a sum of multiple sinusoidal pulses ( $\sum_{n=1}^{k} A_n e^{-i(n\omega)t}$ ), through a Fast Fourier Transform (FFT). The result is the frequency spectrum of the heat conduction profile, which can be translated to a pressure spectrum for the air surrounding the particle (Diebold and Westervel, 1988) as shown in Eq. (2). The derivation of Eq. (2) is based on the general OA equation and it is detailed in Appendix A. The expected OA signal is actually the intensity of the pressure wave at the frequency bandwidth of the sound detector.

$$p = i c_S^2 \frac{\beta}{c_p} \sum_{n=1}^k \frac{A_n}{n\omega} e^{-i(n\omega)t}$$
 (2)

In Eq. (2), p is the pressure of the air surrounding the BC particle,  $c_s$  is the speed of sound,  $\beta$  is the air thermal expansion coefficient,  $C_p$  is the air specific heat capacity,  $\omega$  is the modulation angular frequency, and  $A_n$  is the intensity of the n harmonic of the modulation frequency.

#### 115 2.3 Mathematical description of the model

To calculate the particle's absorption coefficient, (Hadef et al., 2010) relied on the experimental data of Krishnan et al. (2000) for estimating the  $E_m$  parameter. Instead, we calculate the absorption coefficient based on the Mie theory for spherical particles (Hinds, 1999). Specifically, the refractive index of BC particles that was suggested by Bond & Bergstrom (2006), the particle size, and a wavelength range are inputs to the Mie Simulator GUI (2025). This simulator outputs the absorption efficiency of the particle as a function of light wavelength and runs for various particle sizes in the range of 10 to 1000 nm. For validation, the new absorption calculation method was tested with the conditions of Hadef et al. (2010) and produced similar results for the same input. The advantage of the new method is that it can predict the response of particles of different refractive index, without necessitating experimentally determined information.

The particle heat conduction term has been described by different models, as outlined by Liu et al. (2006). The Boundary-Sphere Method is used here as a good compromise between accuracy and complexity. Key to this analysis is the particle Knudsen number (Kn). The volume around the particle is split into two regions, one close to the particle where heat conduction from the particle to the boundary sphere takes place in the free-molecular regime (Kn > 1), and an outer region where heat from the boundary sphere to the surrounding air dissipated in the continuum regime (Kn < 1). The boundary sphere is assumed to have a uniform temperature ( $T_{\delta}$ ) and its radius is equal to the radius of the particle plus a parameter  $\delta$ .

According to model formulation, heat conduction terms in the free-molecular and continuum regimes must be equal. This condition is used to calculate the  $\delta$  and  $T_{\delta}$  terms by an iterative process. An initial estimate of  $T_{\delta}$  is first given and the values of mean free path and Kn for the given particle are calculated, while the parameter  $\delta$  is approximated. The free molecular (Eq. 3) and the continuum (Eq. 4) heat conduction rates are then determined. The initial value of  $T_{\delta}$  of the Boundary Sphere is corrected based on the difference between the two heat conduction rates. If the continuum heat conduction rate is larger than



155

160



the free molecular one, then  $T_{\delta}$  is reduced based in Eq. (5) and vice versa. The process terminates when the correction on  $T_{\delta}$  between two iterations is lower than  $1e^{-6}$  K.

$$\dot{Q}_{fm} = a_{th} \frac{\pi D^2}{4} \frac{p_g}{2} \sqrt{\frac{8k_B T_{\delta}}{\pi m_g}} \frac{\gamma^* + 1}{\gamma^* - 1} \left( \frac{T_p}{T_{\delta}} - 1 \right)$$
(3)

$$\dot{Q}_c = 4\pi (\frac{D}{2} + \delta) \int_{T_a}^{T_\delta} k_g dT \tag{4}$$

$$T_{\delta,i+1} = T_{\delta,i} + f_c(\dot{Q}_{fm} - \dot{Q}_c) \tag{5}$$

In Eq. (3),  $a_{th}$  is the thermal accommodation coefficient for heat conduction from the particle to air, D is the particle's diameter,  $p_g$  is the pressure of the surrounding air,  $k_B$  is the Boltzmann constant,  $m_g$  is the average mass of a gas molecule,  $\gamma^*$  is the average specific heat ratio of air for large  $\Delta T$ ,  $T_p$  is the particle temperature and  $T_{\delta}$  is the air temperature in the small layer around the particle with radius  $\delta$ . In Eq. (4),  $k_g$  is the air specific heat coefficient and  $T_g$  is the air temperature.

Finally, parameter  $f_c$  in Eq. (4) is a convergence factor with significant implications on the proper performance of the algorithm. Too large values may lead to divergence of the simulation while too small values may cause the algorithm to be very slow. The terms  $\dot{Q}_{fm}$  and  $\dot{Q}_c$  are of the same order of magnitude as the absorption term, which increases with particle volume. That could lead to large  $\Delta T_{\delta}$  between iterations and thus divergence for large particles, which exhibit high absorption rates, if  $f_c$  is the same in all cases. Thus, the parameter  $f_c$  is set to be inversely proportional to particle volume (D<sup>3</sup>), so that the model can be used for a wide range of particle diameters without adjustment.

For applying the model to agglomerate particles rather than perfect spheres (Imran and Hochgreb, 2019), we use the diameter of gyration  $D_g$  as shown in Eq. (6).

$$D_g = d_{pp} \left(\frac{N_p}{k_f}\right)^{1/D_f} \tag{6}$$

where,  $d_{pp}$  is the diameter of the primary particles (spherules) that form the agglomerate,  $N_p$  is the number of primary particles in the agglomerate,  $k_f$  is fractal pre-factor and  $D_f$  is the fractal dimension which determines the shape of the particle. A fractal dimension equal to 1 means that the agglomerate has the shape of a line, while a value equal to 3 is representative of a sphere.

There are some implications related to the absorption and conduction terms when modelling particles as agglomerates. Starting with the absorption term, the approach of the RDG model is taken (Bond and Bergstrom, 2006). First, total absorption is equal to the absorption of a primary particle, based on the Mie theory (Hinds, 1999), multiplied by the number of primary particles  $(N_p * Q_{abs} \frac{\pi d_{pp}^2}{4})$ . This means than an agglomerate particle comprised of e.g. 100 primary particles, absorbs the same amount of light as 100 distinct spherical particles of the same size as the primary particles. This is valid as the diameter of primary particles that form typical agglomerate BC particles is much smaller than the excitation light wavelength, typically in the visible or near-infrared ranges (400 – 900 nm). With this approach, the light can miss the front part of the agglomerate and be absorbed by the rear part or the inner part of the agglomerate. Mathematically, this is expressed by the absorption efficiency





of Mie theory which is linearly dependent on particle diameter for  $d_{pp} < 150 \, nm$  and wavelengths in the visible spectrum (Jennings and Pinnick, 1980). The result is that the absorption of the particle is proportional to the total volume of the agglomerate, independently of its shape.

In the heat conduction term, the diameter of the spherical particle is replaced by the diameter of gyration of the agglomerate particle  $(D_g)$ , as presented in Eq. (6). The diameter of gyration is a proxy of the wetted surface of the particle, which is relevant for heat conduction. For the internal energy term, the total mass of the particles is used, which is equal to the volume of each primary particle  $(\frac{\pi d_{pp}^3}{6})$  multiplied by the number of primary particles in the agglomerate  $(N_p)$  and the bulk material density  $(\rho_{BC})$ .

#### 2.4 Agglomerate particle relaxation time

The thermal relaxation time of a spherical particle can be calculated on the basis of Eq. (1) as shown in Starke et al. (2003). We use a similar approach for agglomerate particles. With the light source off, the absorption term is set equal to zero, further to the radiation and sublimation terms, leaving only the internal energy and the heat conduction terms in the energy balance equation – Eq. (7). The heat conduction term is expressed for the free molecular regime. The result is a differential equation, with internal energy depending on the first derivative of particle temperature, and heat conduction being linearly dependent on particle temperature. In the left side of Eq. (7),  $\rho_{BC}$  is material density and  $C_{BC}$  is the specific heat capacity of the particle. The particle temperature is given as exponential function of time (Eq. 8) with the relaxation time being the inverse of the exponent parameter, as shown in Eq. (9). The Volume-to-Surface ratio for the agglomerate particle is defined in Eq. (10).

$$\rho_{BC}C_{BC}N_{p}\frac{\pi d_{pp}^{3}}{6}\frac{dT_{p}}{dt} = -a_{th}\frac{\pi D_{g}^{2}}{4}\frac{p_{g}}{2}\sqrt{\frac{8k_{B}T_{\delta}}{\pi m_{g}}}\frac{\gamma^{*}+1}{\gamma^{*}-1}\left(\frac{T_{p}}{T_{g}}-1\right) \tag{7}$$

$$T = T_0 e^{-at} (8)$$

$$t_{rel} = \frac{1}{a} = \frac{\rho_p c_p}{a_{th}} \frac{Volume}{Surface} \frac{4}{3P_g} \sqrt{\frac{\pi T_g}{8R}} \frac{\gamma^* - 1}{\gamma^* + 1}$$

$$\tag{9}$$

$$85 \quad \frac{Volume}{Surface} = \frac{N_p d_{pp}^3}{D_q^2} \tag{10}$$

#### 3 Results

190

The model presented is used to demonstrate the impact of particle morphology and physical properties on the generated OA and OT signals. To do so, we first outline the relative importance of each dissipation term in Eq. (1). Then, the model is validated by comparing the intensity of the OA signal with experimental results for various light modulations. Finally, the model is applied to demonstrate the effect of different particle properties on the generated signal, depending on light modulation.



200



# 3.1 Light intensity and dissipation mechanisms

Figure 2 shows the importance of each dissipation mechanism in Eq. (1) for a rectangular modulation pulse with 100 kHz frequency, 1 % duty cycle and for various light beam intensities. The resulting pulse duration is 10 ns. The small pulse duration is necessary to evaluate high laser intensities without vaporizing the entire BC particle. The analysis is performed for 50 nm spherical BC particles. For laser intensities larger than  $10^{3.8}$  W/mm², the heat dissipated by conduction starts to decrease with an almost mirroring increase of the radiation term. For intensities larger than about  $10^4$  W/mm², sublimation rapidly increases and becomes the prevailing mechanism. One may conclude that laser intensities between  $10^{3.8}$  and  $10^4$  W/mm² are suitable for LII applications, as a large share of the energy is dissipated through radiation. Intensities closer to  $10^{3.8}$  W/mm² should actually be preferred to reduce the destruction of particles due to sublimation.

Lower laser intensities are optimal for OA and OT applications as all the energy is dissipated through heat conduction, which is the generative term for producing instrument response with both techniques. Intensities up to  $10^3 \, \text{W/mm}^2$  are appropriate, however intensities below  $10^2 \, \text{W/mm}^2$  are still adequate and need a less powerful light source. For longer pulses, radiation and sublimation require lower light intensity, because more time is given for particle temperature increase.

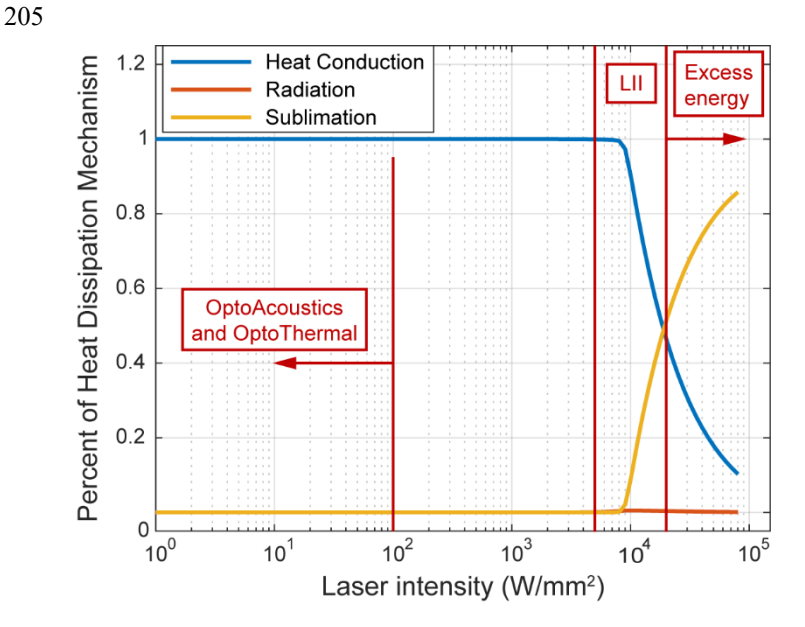


Figure 2: The three main dissipation mechanisms (heat conduction with blue, radiation with orange and sublimation with yellow) as a function of light intensity, in the range  $1 - 10^5$  W/mm<sup>2</sup> (example for 50 nm spherical particles).

# 3.2 Model validation

The model is first validated by comparing the values of the individual terms of the energy balance model against the literature values of Hadef et al. (2010), who included all dissipation mechanisms, and Snelling et al. (2004) who only considered conduction (Table 1). However, the latter is very suitable to an OA application of LII models, as it uses low-fluence light



225

230

235



beams to fine-tune the conduction term. Validation is done using the same values in our study and the literature models for particle size and morphology, air temperature and light wavelength, intensity and modulation. Our model predicts identical particle temperature profiles to Snelling et al. (2004). Compared to Hadef et al. (2010), conduction and radiation profiles seem identical. Sublimation and decrease of particle diameter are slightly underestimated by our model. Since the laser intensity of OA sensors is several orders of magnitude lower than the one required to produce sublimation, our model can be considered adequately validated.

Table 1: Comparison of the particle temperature and the intensity of dissipation mechanism as predicted by our model to the same metrics predicted by the models of Hadef et al. (2010) and Snelling et al. (2004) for the same input parameters.

	Hadef et al.	Snelling et al.	This study
Peak Temperature [K]	-	~ 2950 K	2933 K
Temperature after 800 ns [K]	-	~ 2320 K	2316 K
Peak Absorption [10 <sup>-5</sup> W]	2	=	3
Peak Conduction [nW]	70	=	85
Peak Radiation [nW]	6	=	6
Peak Sublimation [10 <sup>-5</sup> W]	3	=	3
Conduction after 800 ns [nW]	11	-	12
Radiation after 800 ns [nW]	0.11	- -	0.12
Sublimation after 200 ns [nW]	4	- -	1
Diameter after 800 ns [nm]	17	<del>-</del>	18

The complete model validation is conducted by comparing the model output with experimental data while varying the modulation duty cycle. Correctly predicting the effects of the duty cycle impact means that all components of the model (absorption, heat dissipation and OA signal) are represented correctly in the model.

For the validation, we run simulations with 100 kHz modulation frequency and a rectangular pulse with the duty cycle varying between 1 % and 50 %. The sample comprised 20 nm spherical BC particles. Figure 3 depicts the main processes of our model for the 1 % duty cycle (Fig.3a-d) and the 50 % duty cycle (Fig.3e-h). Figures 3a,e first show the profile of absorbed energy for the two cases. This has a perfect rectangular pulse, identical to the excitation pulse. Then, Fig. 3b,f show the profile of heat conduction from the particle to the surrounding air. For the short pulse, the heat conduction linearly increases while the light is on, and drops exponentially afterwards. Instead, for the long duty cycle, heat conduction stabilizes at the level of the absorption power after approximately 1 µs and falls exponentially after the light source is turned off. Figures 3c,g show the frequency response of the conduction profile of Fig. 3b,f respectively, as calculated by a Fast Fourier Transform. Figures 3d,h show the frequency response of the acoustic wave, which is calculated from the frequency response of heat conduction following Eq. (2).



245



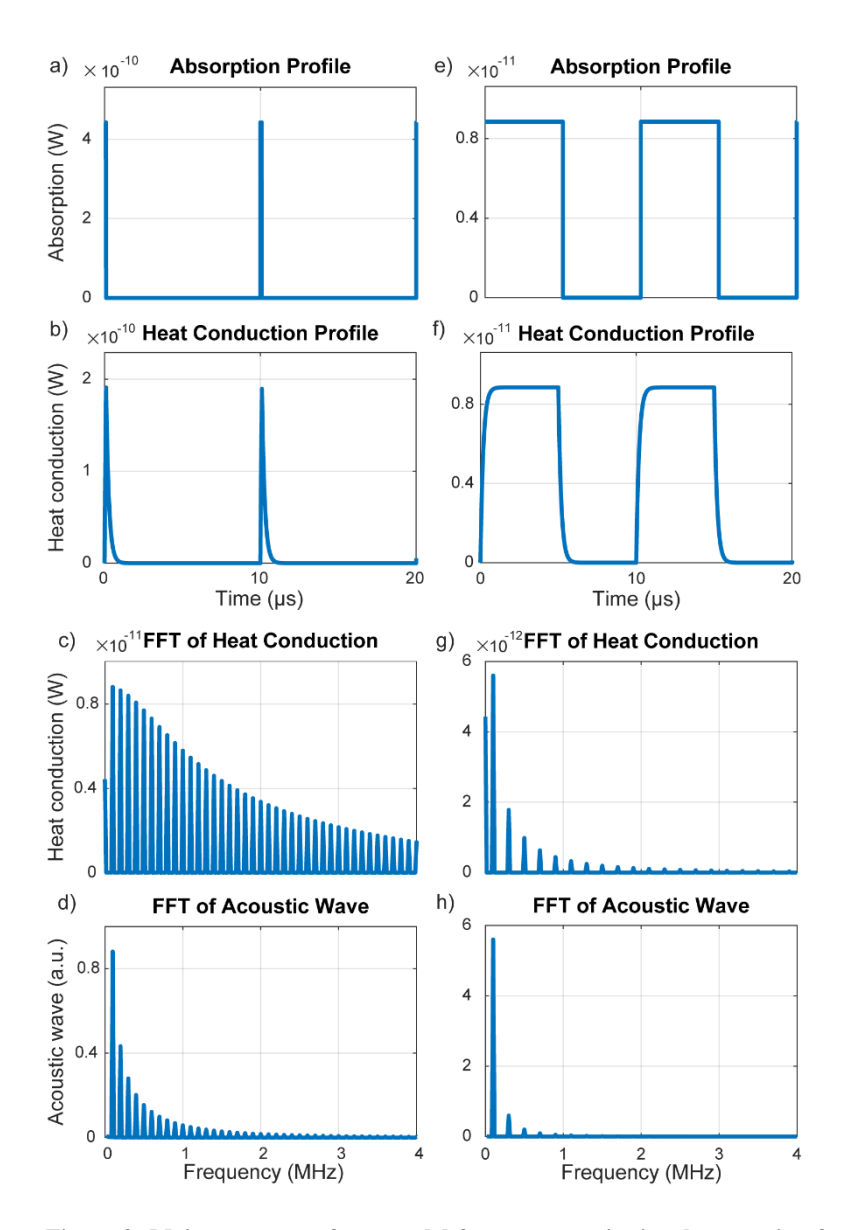


Figure 3: Main processes of our model for optoacoustic signal generation for 1 % (3a-d) and 50 % duty cycle (e-h). From top to bottom, the panels show the profile of light absorption by the particle (a, e), heat conduction from the particle (b, f), FFT of the heat conduction profile (c, g), and FFT of the acoustic wave (d, h).

For the experimental validation of the model, we used the low-cost optoacoustic sensor that we previously presented in Stylogiannis et al. (2021), but with a different laser source (FBLD-450-0.800W-FC105-BTF) that allowed us to vary the duty cycle from 2 % to 50 %. A powermeter was used to correct the response of the sensor for any deviations of the laser power. The power corrected OA response of a rectangular pulse with varying duty cycle is shown in Fig. 4 (dots) along with the model predictions (line), using the model previously developed. The response of each duty cycle was normalized based on the response for the 50 % duty cycle. Figure 4 shows that the model can predict the normalised impact of the duty cycle on the





signal, with great accuracy compared to the experimental findings. Very small deviations are observed primarily for small duty cycles. From such results, we conclude that the model can be used for accurate estimations of signal modulation profile on OA sensors.

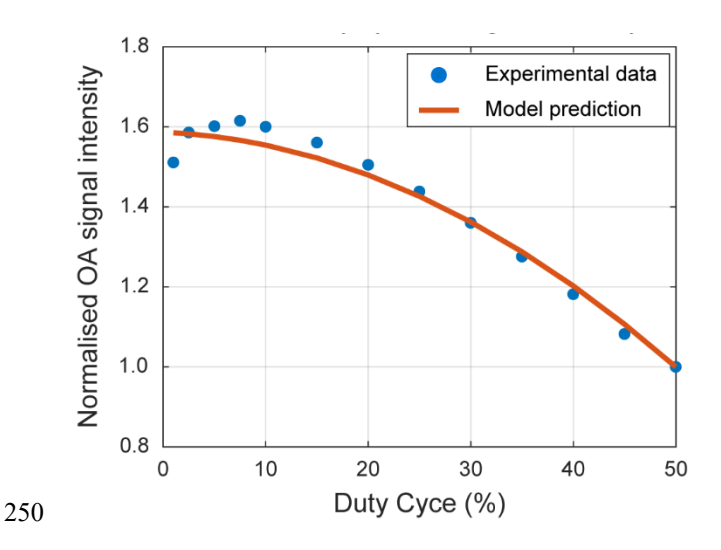


Figure 4: Validation of the model with experimental data, having the laser duty cycle as an independent variable of the model.

#### 3.3 Effect of particle morphology on OA signal

Next, we proceed to examine the intensity of the generated OA signal for various particle properties. Heat flux (W) generally increases with particle size due to larger mass and surface area. Hence, to make the results easier to interpret, we present the ratio of heat conduction over particle mass (W/kg) for any particle, normalised over the same magnitude of a 20 nm spherical particle. This newly introduced metric is called normalised signal intensity. We assume that all particles have the same mass absorption coefficient (MAC), thus any possible combination of particle morphology and laser modulation should ideally produce a value of one expressed in this normalised signal intensity. We will show that this is not always true.

The morphology of the agglomerate particle on generated signal is first examined. The gyration diameter is varied between 100 nm and 200 nm, the primary particle size between 25 nm and 40 nm and the fractal dimension between 1.2 and 2.8 (Olfert and Rogak, 2019). A sinusoidal pulse is used with a modulation frequency of 100 kHz. The wavelength of the light beam is 450 nm and its intensity is 10 W/mm<sup>2</sup>. The light wavelength does not affect the performed analysis, as the wavelength is not relevant for the heat dissipated from the particle.



275

280



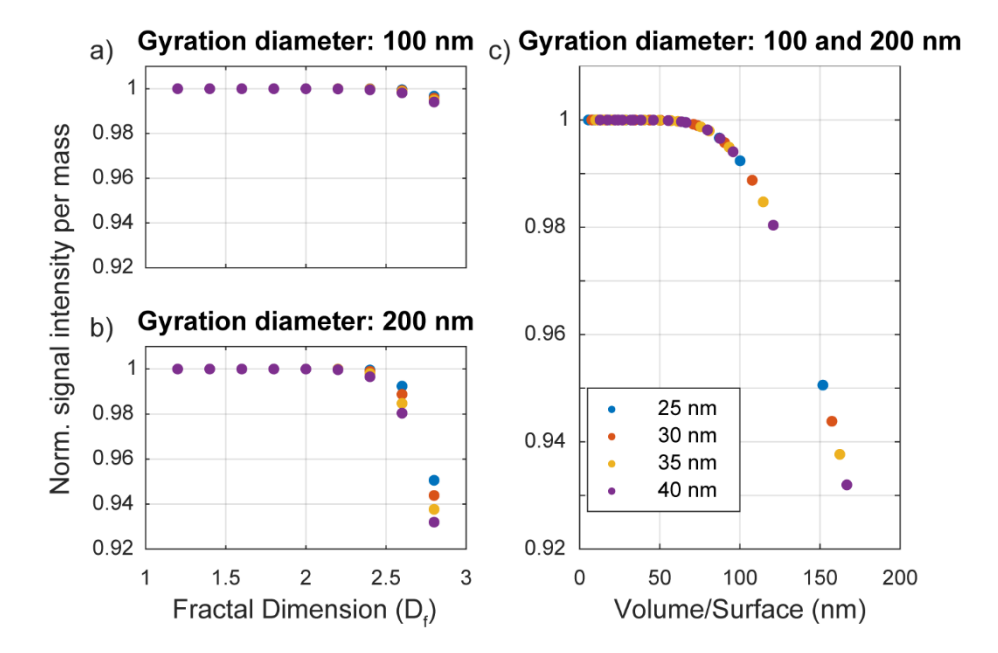


Figure 5: (a,b) Normalized signal intensity per mass as a function of the fractal dimension for particles with primary particle size ranging from 25 to 40 nm and diameter of gyration (a) 100 nm and (b) 200 nm; (c) Normalized signal intensity per mass as a function of the particle Volume to Surface ratio for all particle diameters.

Figures 5a,b show that the normalized signal intensity for 100 nm and 200 nm agglomerate particles, having the size of primary particles as the model parameter. The normalized signal intensity drops as the fractal dimension increases. Actually, the drop is larger as particle size increases and is differentiated according to primary particle size. However, this correlation is different for each diameter of gyration, proving that the fractal dimension alone is not a good predictor of the normalised signal intensity. In Fig. 5c, the data for both diameters of gyration are plotted over the volume to surface ratio (V/S) of the agglomerate particle on the x axis. We observe that all particles fall in the same line, independently of their diameter of gyration and primary particle size. Thus, the V/S ratio can be used to correct the OA signal for particles of different morphology, instead of the diameter of gyration or the fractal dimension.

## 3.4 Effect of particle physical properties

Previously, we showed that the V/S ratio of agglomerate particles can be used to predict the normalised signal intensity for particles of different morphology. The relevance of the V/S ratio can potentially be further generalized by looking at whether this can be used to predict responses when other parameters are varied. We first examined the impact of particle physical properties, and specifically the density ( $\rho_{BC}$ ), the specific heat capacity ( $C_{BC}$ ), and the thermal accommodation coefficient ( $a_{th}$ ). These three parameters are included in Eq. (9) for the particle's relaxation time in the  $\frac{\rho_{BC}C_{BC}}{a_{th}}$  ratio. This ratio is analogous to the inverse thermal diffusivity of the particle. The nominator is equal to the amount of energy that the particle can store, while the denominator denotes how good is the particle at dissipating this energy through heat conduction. Instead of independently





varying each parameter, this ratio is varied directly within a much broader range than the one expected for freshly generated BC particles.

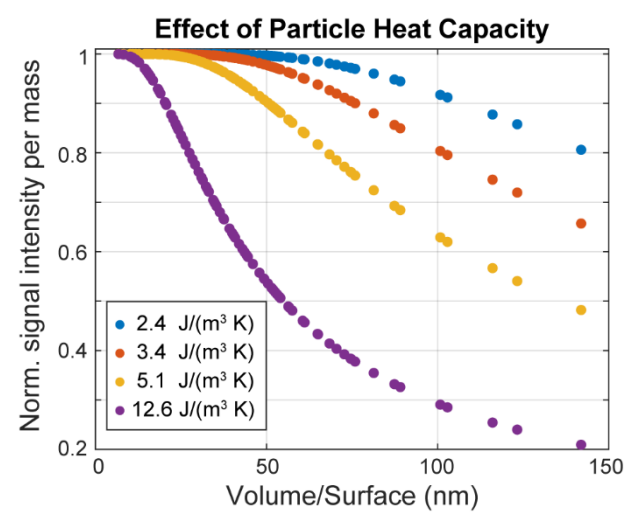


Figure 6: Impact of particle physical properties on signal intensity as a function of the volume-to-surface ratio.

Figure 6 shows that the physical properties have a large effect on the normalised signal intensity per mass. The larger the density and the heat capacity and the smaller the heat accommodation coefficient, the lower the normalised signal intensity.

This finding indicates that for particles with known V/S ratio, the signal decrease can be used to extract information about the particle's physical properties. This way, BC can be distinguished from other absorbing particles of different properties, for example ash particles.

# 3.5 Effect of light modulation

The impact of the modulation frequency of the excitation light on the signal is examined by varying the frequency in the range from 100 kHz to 500 kHz. Relatively high frequencies are examined for demonstration because these are expected to lead to larger deviations, even though conventional sensors typically use much lower frequencies.





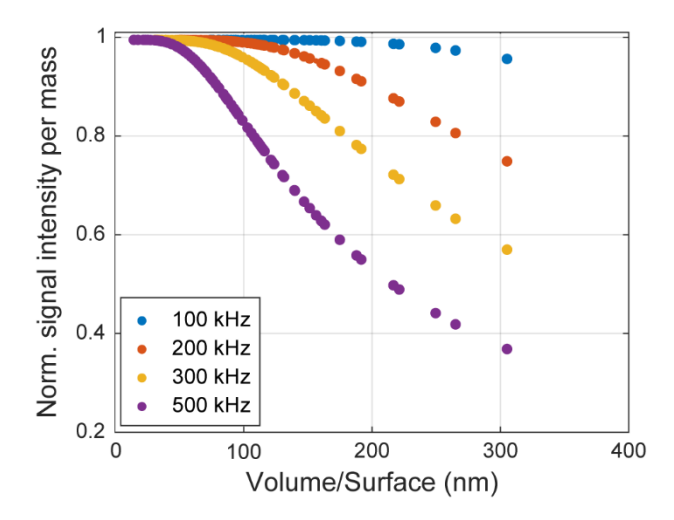


Figure 7: Impact of light modulation frequency on signal intensity as a function of the volume-to-surface ratio.

Figure 7 shows that the modulation frequency significantly affects the normalised signal intensity per mass, even when the particle V/S is used as the independent variable. A clear trend is seen with higher frequencies leading to signal drop, even for small V/S values. This is because the particle is not given enough time to cool as frequency increases. We can use the finding of Fig. 7 in order to harmonize measurements from different instruments that use different modulation frequency, if the V/S ratio of sample particles is known or can be estimated.

#### 3.6 Particle relaxation time

The outcome of this analysis is that the V/S ratio has some predictive value for the normalised signal intensity, but it cannot be used to normalize the signal from devices of different operation characteristics (modulation frequency) or to correct for particle properties. In search of a more general metric, the relaxation time of the particle can be proposed as a reliable metric since it includes the volume to surface ratio and the  $\frac{\rho_{BC}C_{BC}}{a_{th}}$  ratio. To further generalize it and include the modulation frequency, we introduce a dimensionless characteristic metric (TOA) equal to the product of the relaxation time and the modulation frequency, as shown in Eq. (11).

$$T_{OA} = t_{rel} f_{mod} \tag{11}$$





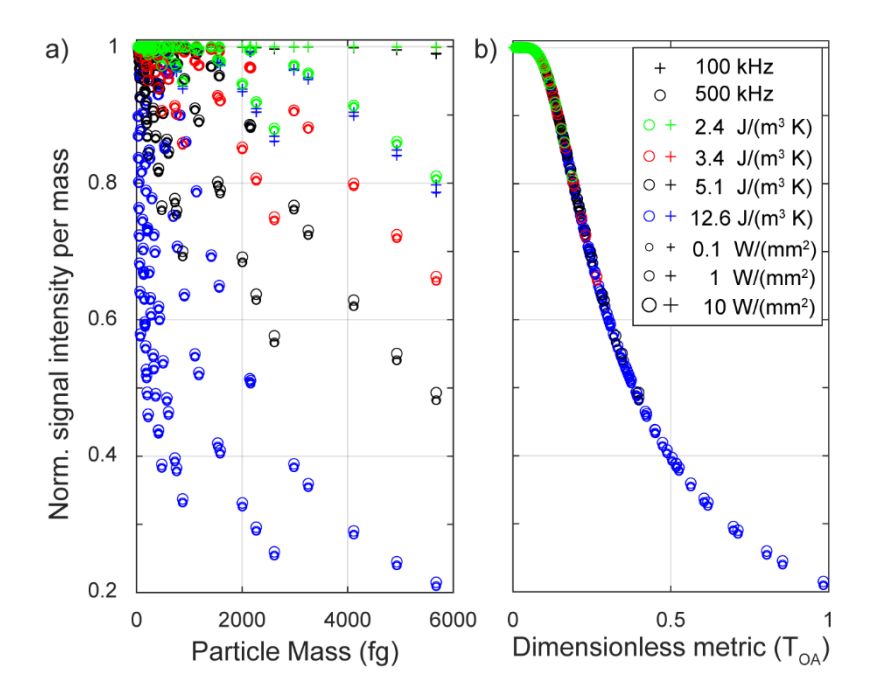


Figure 8: Normalized signal intensity per mass for various particles and for different combinations of modulation frequency, particle physical properties and laser intensity as a function of a) particle mass and b) dimensionless time.

Figure 8 shows the normalised signal for all variables examined in the current study, for particles Kn >>1. Similar patterns can be calculated for Kn = 1 and larger. In Fig. 8a, the normalised signal is shown as a function of particle mass. We deduce that there can be large variance in the normalised signal due to variance in particle physical properties and morphology even if the particles have the same refractive index and MAC. In contrast, Fig. 8b shows that when the dimensionless metric is used as independent variable, then all values fall in the same line, demonstrating the excellent predictive value of the proposed metric. For values of TOA less than 0.1 (i.e. modulation period is ten times the particle's relaxation time) we observe that the normalised signal intensity is equal to 1, while for larger values it drops down to 0.2 when the particle relaxation time is equal to the modulation period.

The curve in Fig. 8b is valid for OA sensors with sinusoidal modulation or rectangular pulses with 50 % duty cycles. For rectangular pulses with different duty cycles some modifications are required to use the same curve. Specifically, for OA sensors the curve must be corrected based on the signal intensity factor that is shown on Fig. 4.

# 4 Discussion

325

The proposed model can be used for various applications, including the design of OA sensors and the harmonization of measurements from different instruments. The first outcome of the current analysis is that the signal can vary even for particles with the same refractive index and the same MAC when particle morphology and other particle physical properties vary.



330

335

340

345

350

355

360



Physically, the cooling efficiency of particles of same mass is the determinant variable for the signal intensity when MAC is constant. The temperature of the particle increases when the light is on. The heat that it accumulates during this phase depends only on its MAC and its mass. The cooling of the particle depends on both its physical and morphological parameters. If the relaxation time is long, the cooling process is slow, and the particle may not have enough time to reach its initial temperature, especially for high modulation frequencies. The same amount of energy is conducted compared to a particle with short relaxation time, but the amplitude of transient term of the heat flux is smaller, and this results in a weaker signal (decreased normalised signal to mass ratio). The above mechanism is the explanation why the product of relaxation time with modulation frequency is so effective in predicting the phenomenon. The available time for particle cooling must be at least 10 times larger than the particle relaxation time to avoid signal reduction.

Current sensors typically use modulation frequencies lower than 10 kHz. In addition, BC particles do not vary that much in their physical properties while their fractal dimension is typically below 2.5. All these parameters combined result in minimum deviations between instruments in most, if not all, practical cases, at least for BC particles. However, for special cases some deviations may be observed even with current sensors. A typical example is tarballs (also called BrC spheres) that are produced from biomass burning and combustion in marine engines (Adler et al., 2019; Corbin et al., 2019). These are strong absorbing carbonaceous particles that have an amorphous instead of an agglomerate shape. What makes tarballs even more interesting is the inability to measure them with LII instruments, as they do not incandesce (Adler et al., 2019). A tarball of 150 nm, measured by an OA instrument with modulation frequency 100 kHz will be detected with an efficiency of 72 % compared to conventional BC particles that would be 100 % visible. This would result in a 28 % underreporting of the tarball mass concentration. An OA sensor that utilizes the findings of the current work, can accurately measure tarballs concentration and potentially distinguish them from conventional BC particles.

Finally, new systems can be specifically designed to take advantage of this non-linear relation between absorption and conduction. An enhanced OA system would be able to simultaneously measure the intensity and time delay (phase) of the sound. The time delay can be correlated to the particle relaxation time. This was already demonstrated for BC agglomerates and spherical nigrosine particles by Ajtai et al. (2023), who showed a correlation between the particle size and the signal phase. Similar effects of BC particles morphology on the generated signal are expected for OT sensors. A modified version of the presented model that considers the physics of interferometry and utilizes low modulation frequencies can provide useful insight got OT sensors design. Precisely due to the much lower modulation frequencies that are used by OT systems, the effects are expected to be visible in the time domain and not the frequency domain.

#### **Author Contribution**

Nikolaos Kousias: Conceptualization, Methodology, Software, Visualization, Formal analysis and Writing - original draft, Ioannis Raptis: Conceptualization, Validation, Writing - review and editing, Linda Haedrich: Conceptualization, Validation, Writing - review and editing, Vasilis Ntziachristos: Funding acquisition and Writing - review and editing, Leonidas Ntziachristos: Supervision, Funding acquisition and Writing - review and editing.





# **Competing interests**

The authors declare that they have no conflict of interest.

## 365 Acknowledgements

We would like to thank Antonios Stylogiannis for his contribution in the development of the concepts that are presented in this work. We acknowledge open-source software resources offered by the Virtual Photonics Technology Initiative, at the Beckman Laser Institute, University of California, Irvine.

#### **Financial Support**

This work received funding from the European Union's Horizon 2020 research and innovation programme under grant agreement No 862811 (RSENSE).

#### References

375

- Adler, G., Wagner, N. L., Lamb, K. D., Manfred, K. M., Schwarz, J. P., Franchin, A., Middlebrook, A. M., Washenfelder, R. A., Womack, C. C., Yokelson, R. J., and Murphy, D. M.: Evidence in biomass burning smoke for a light-absorbing aerosol with properties intermediate between brown and black carbon, Aerosol Science and Technology, 53, 976–989, https://doi.org/10.1080/02786826.2019.1617832, 2019.
  - Ajtai, T., Hodovány, S., Schnaiter, M., Szabó, G., and Bozóki, Z.: Absorption based size characterisation of aerosol by using photoacoustic spectroscopy, Atmos Environ, 304, 2–6, https://doi.org/10.1016/j.atmosenv.2023.119772, 2023.
- Baumann, B., Wolff, M., Kost, B., and Groninga, H.: Finite element calculation of photoacoustic signals, Appl Opt, 46, 1120–1125, https://doi.org/10.1364/AO.46.001120, 2007.
  - Bond, T. C. and Bergstrom, R. W.: Light absorption by carbonaceous particles: An investigative review, Aerosol Science and Technology, 40, 27–67, https://doi.org/10.1080/02786820500421521, 2006.
  - Bond, T. C., Doherty, S. J., Fahey, D. W., Forster, P. M., Berntsen, T., Deangelo, B. J., Flanner, M. G., Ghan, S., Kärcher, B., Koch, D., Kinne, S., Kondo, Y., Quinn, P. K., Sarofim, M. C., Schultz, M. G., Schultz, M., Venkataraman, C., Zhang, H.,
- Zhang, S., Bellouin, N., Guttikunda, S. K., Hopke, P. K., Jacobson, M. Z., Kaiser, J. W., Klimont, Z., Lohmann, U., Schwarz, J. P., Shindell, D., Storelvmo, T., Warren, S. G., and Zender, C. S.: Bounding the role of black carbon in the climate system: A scientific assessment, Journal of Geophysical Research Atmospheres, 118, 5380–5552, https://doi.org/10.1002/jgrd.50171, 2013.
  - Coalition, C. A.: Marine Black Carbon Emissions: Identifying Research Gaps, 1–17 pp., 2014.
- 390 Corbin, J. C., Czech, H., Massabò, D., de Mongeot, F. B., Jakobi, G., Liu, F., Lobo, P., Mennucci, C., Mensah, A. A., Orasche, J., Pieber, S. M., Prévôt, A. S. H., Stengel, B., Tay, L. L., Zanatta, M., Zimmermann, R., El Haddad, I., and Gysel, M.: Infrared-





- absorbing carbonaceous tar can dominate light absorption by marine-engine exhaust, NPJ Clim Atmos Sci, 2, https://doi.org/10.1038/s41612-019-0069-5, 2019.
- Cotterell, M. I., Ward, G. P., Hibbins, A. P., Haywood, J. M., Wilson, A., and Langridge, J. M.: Optimizing the performance of aerosol photoacoustic cells using a finite element model. Part 1: Method validation and application to single-resonator multipass cells, Aerosol Science and Technology, 53, 1107–1127, https://doi.org/10.1080/02786826.2019.1650161, 2019.
  - Diebold, G. J. and Westervel, P. J.: The photoacoustic effect generated by a spherical droplet in a fluid, Journal of the Acoustical Society of America, 84, 2245–2251, https://doi.org/10.1121/1.397017, 1988.
- Dou, T. F. and Xiao, C. De: An overview of black carbon deposition and its radiative forcing over the Arctic, Advances in Climate Change Research, 7, 115–122, https://doi.org/10.1016/j.accre.2016.10.003, 2016.
  - Fujii, H., Terabayashi, I., Kobayashi, K., and Watanabe, M.: Modeling photoacoustic pressure generation in colloidal suspensions at different volume fractions based on a multi-scale approach, Photoacoustics, 27, 100368, https://doi.org/10.1016/j.pacs.2022.100368, 2022.
- Hadef, R., Geigle, K. P., Meier, W., and Aigner, M.: Soot characterization with laser-induced incandescence applied to a laminar premixed ethylene–air flame, International Journal of Thermal Sciences, 49, 1457–1467, https://doi.org/10.1016/J.IJTHERMALSCI.2010.02.014, 2010.
  - Hinds, W. C.: Aerosol technology: properties, behavior, and measurement of airborne particles, 2nd ed., New York (N.Y.): Wiley, 1999.
- Imran, H. and Hochgreb, S.: Modelling of Photoacoustic Signal from Spherical and Fractal Aerosols in the Transition and Continuum Regimes, 5306, 2019.
  - Janssen, N. A. H., Hoek, G., Simic-Lawson, M., Fischer, P., van Bree, L., Brink, H. Ten, Keuken, M., Atkinson, R. W., Ross Anderson, H., Brunekreef, B., and Cassee, F. R.: Black carbon as an additional indicator of the adverse health effects of airborne particles compared with pm 10 and pm 2.5, Environ Health Perspect, 119, 1691–1699, https://doi.org/10.1289/ehp.1003369, 2011.
- Jennings, S. G. and Pinnick, R. G.: Relationships between visible extinction, absorption and mass concentration of carbonaceous smokes, Atmospheric Environment (1967), 14, 1123–1129, https://doi.org/10.1016/0004-6981(80)90176-6, 1980.
  - Kosterev, A. A., Mosely, T. S., and Tittel, F. K.: Impact of humidity on quartz-enhanced photoacoustic spectroscopy based detection of HCN, Appl Phys B, 85, 295–300, https://doi.org/10.1007/s00340-006-2355-2, 2006.
- 420 Krishnan, S. S., Lin, K.-C., and Faeth, G. M.: Optical Properties in the Visible of Overfire Soot in Large Buoyant Turbulent Diffusion Flames, J Heat Transfer, 122, 517–524, https://doi.org/10.1115/1.1288025, 2000.
  - Liu, F., Daun, K. J., Snelling, D. R., and Smallwood, G. J.: Heat conduction from a spherical nano-particle: Status of modeling heat conduction in laser-induced incandescence, Appl Phys B, 83, 355–382, https://doi.org/10.1007/s00340-006-2194-1, 2006.



440



- Meyer, T. R., Halls, B. R., Jiang, N., Slipchenko, M. N., Roy, S., and Gord, J. R.: High-speed, three-dimensional tomographic laser-induced incandescence imaging of soot volume fraction in turbulent flames, Opt Express, 24, 29547, https://doi.org/10.1364/oe.24.029547, 2016.
  - Michelsen, H. A.: Understanding and predicting the temporal response of laser-induced incandescence from carbonaceous particles, Journal of Chemical Physics, 118, 7012–7045, https://doi.org/10.1063/1.1559483, 2003.
- Michelsen, H. A., Schulz, C., Smallwood, G. J., and Will, S.: Laser-induced incandescence: Particulate diagnostics for combustion, atmospheric, and industrial applications, Prog Energy Combust Sci, 51, 2–48, https://doi.org/10.1016/j.pecs.2015.07.001, 2015.
  - Moosmüller, H., Chakrabarty, R. K., and Arnott, W. P.: Aerosol light absorption and its measurement: A review, J Quant Spectrosc Radiat Transf, 110, 844–878, https://doi.org/10.1016/j.jqsrt.2009.02.035, 2009.
- Olfert, J. and Rogak, S.: Universal relations between soot effective density and primary particle size for common combustion sources, Aerosol Science and Technology, 53, 485–492, https://doi.org/10.1080/02786826.2019.1577949, 2019.
  - Pustovalov, V. K.: Light To Heat Conversion and heating of single nanoparticles, their assemblies, and the surrounding medium under pulses, RSC Adv., 6, 81266–81289, 2016.
  - Snelling, D. R., Liu, F., Smallwood, G. J., and Gülder, Ö. L.: Determination of the soot absorption function and thermal accommodation coefficient using low-fluence LII in a laminar coflow ethylene diffusion flame, Combust Flame, 136, 180–
- Starke, R., Kock, B., and Roth, P.: Nano-particle sizing by laser-induced-incandescence (LII) in a shock wave reactor, Shock Waves, 12, 351–360, https://doi.org/10.1007/s00193-003-0178-1, 2003.
  - Stylogiannis, A., Kousias, N., Kontses, A., Ntziachristos, L., and Ntziachristos, V.: A low-cost optoacoustic sensor for environmental monitoring, Sensors (Switzerland), 21, 1–14, https://doi.org/10.3390/s21041379, 2021.
- 445 Mie Simulator GUI: https://github.com/VirtualPhotonics/MieSimulatorGUI, last access: 9 September 2025.

190, https://doi.org/10.1016/J.COMBUSTFLAME.2003.09.013, 2004.

- Willems, R. C., Bakker, P. C., and Dam, N. J.: Laser-induced incandescence versus photo-acoustics: implications for qualitative soot size diagnostics, Appl Phys B, 125, 1–9, https://doi.org/10.1007/s00340-019-7248-2, 2019.
- World Health Organization: Health effects of black carbon, Available at: http://hdl.handle.net/20.500.11822/8699 (Accessed: 8 March 2022), 2012.
- Wysocki, G., Kosterev, A. A., and Tittel, F. K.: Influence of molecular relaxation dynamics on quartz-enhanced photoacoustic detection of CO2 at λ = 2 μm, Appl Phys B, 85, 301–306, https://doi.org/10.1007/s00340-006-2369-9, 2006.
  - Zhou, S.: Fully coupled model for frequency response simulation of miniaturized cantilever-based photoacoustic gas sensors, Sensors (Switzerland), 19, https://doi.org/10.3390/s19214772, 2019.





#### 455 Appendix A

470

The basic equation for Optoacoustics with the assumption of thermal confinement is:

$$\left(\nabla^2 - \frac{1}{c_s^2} \frac{d^2}{dt^2}\right) p = -\frac{\beta}{c_p} \frac{dH}{dt} \tag{A1}$$

The driving force for OA signal generation is the time derivative of the heat conduction term. When the light source is modulated with a sinusoidal pulse that term takes the form:

$$460 \quad H = Ae^{-i\omega t} \tag{A2}$$

Assuming that there are no spatial variations of temperature and pressure in the sound source ( $\nabla^2 p = 0$ ) the wave equation in the source takes the form:

$$\frac{d^2p}{dt^2} = -i c_s^2 \frac{\beta}{c_p} A \omega e^{-i\omega t}$$
(A3)

And by integrating we find that the final pressure at the OA source is proportional to:

465 
$$p = i c_s^2 \frac{\beta}{C_p} A \frac{1}{\omega} e^{-i\omega t}$$
 (A4)

It is worth noting that while  $\frac{d^2p}{dt^2}$  is proportional to the frequency of the excitation the final amplitude of the oscillation is inversely proportional to it. An intuitive way to understand that is to think of  $\frac{d^2p}{dt^2}$  as an acceleration term and the final oscillation amplitude as the travelled distance. When the frequency is increased the acceleration is increased proportionally but the available time to travel more distance is decreased proportionally. It can be deduced from Eq. (10) that it is more important for the magnitude of the oscillation to have adequate time rather than high acceleration. The low limit for frequency is the fulfilment of the thermal confinement assumption.

For a rectangular pulse, or for any other Heat Conduction profile, the excitation can be approximated through a Fourier Transform as the sum of sinusoidal pulses with frequency equal to the repetition rate and its harmonics. Mathematically, the excitation, the acceleration, and the distance-oscillation terms for the first k harmonics are expressed in equations (A5) - (A7).

475 
$$H = \sum_{n=1}^{k} A_n e^{-i(n\omega)t}$$
 (A5)

$$\frac{d^2p}{dt^2} = -i c_s^2 \frac{\beta}{c_p} \sum_{n=1}^k A_n(n\omega) e^{-i(n\omega)t}$$
(A6)

$$p = i c_s^2 \frac{\beta}{c_p} \sum_{n=1}^k \frac{A_n}{n\omega} e^{-i(n\omega)t}$$
(A7)